On Supersonic Hydrogen Heating: The TIHTUS Engine

IEPC-2007-57

Presented at the 30th International Electric Propulsion Conference (IEPC)
Florence, Italy, Sep. 11 - 18 2007

Hannah Böhrk* and Monika Auweter-Kurtz†

Institut für Raumfahrtsysteme, Universität Stuttgart
Pfaffenwaldring 31, D–70550 Stuttgart, Germany

boehrk@irs.uni-stuttgart.de

This paper features the intodurction of a variety of probe measurements and the comparison of their measurement results. From total pressure and velocity measurement, under assumption of equilibrium, plasma enthalpy is deduced. For a power input of 50 kW, it yields 450 MJ/kg and compares well to that of 485 MJ/kg derived from plasma power measurements with a cavity calorimeter.

I. Introduction

The current limitations to the exhaust velocity of hydrogen previously heated in a plenum of a rocket engine are imposed for various reasons. At low stagnation pressures, the high bulk enthalpy added, although high, is largely transformed into dissociation and ionisation but cannot be directed to kinetic energy when expanded to lower pressures in a nozzle. Or the bulk enthalpy is, although useful, low at high stagnation pressures. Or, finally, the enthalpy that can be converted to directed kinetic energy at optimum pressure shows a maximum but is a compromise between the two features mentioned above [1]. When both gas temperature and stagnation pressure are increased, the optimum will collide with limitations due to the electrode material. Therefore, new thruster concepts are required in order to produce higher exhaust velocity at high thrust.

A reliable concept is pursued with electric arcjet thrusters. They have been developed since the 1960s [2] and provide relatively high thrust at moderate exhaust velocities. Typical thrust ranges from 0.1 to 6 N for respective power input between 0.75 and 100 kW for the radiation-cooled design. Thrust efficiency is typically below 40% [3]. Currently, the highest exhaust velocities of thermal propulsion concepts that use stationary, chamber-heated hydrogen range between 20 und 25 km/s [2, 3]. An arcjet thruster has a central cathode and an annular anode. The propellant is injected into the ring-shaped gap between the two electrodes and heated up by an electric arc. It is then expanded and accelerated through a nozzle where the energy contained in the plasma is transferred to directed energy. These arcjet characteristics of high specific enthalpy are combined with the presence of a steep radial property gradient as in a hot, energy-rich core with a relatively cold gas layer at its edge. An idea to transfer more power into the plasma flow is to reheat this edge of the plume by another heating mechanism in the way of an afterburner in order not to collide with the material limitations mentioned above. TIHTUS (Thermal-Inductive Hybrid Thruster of the Universität Stuttgart) is a two-stage plasma generator where reheating is realized by means of inductive heating. It has been developed over the past four years [4, 5, 6, 7]. This new concept has the potential to produce large thrust and high effective exhaust velocity by addition of power in the second stage. It is, therefore, considered the predecessor of a future propulsion system for the transport of heavy payload on interplanetary trajectories [4].

The flow from the arcjet plasma generator of TIHTUS is supersonic in its center. From an isentropic consideration of the conservation equations, it can be shown that heating of any supersonic flow has a decelerating effect on the flow [8]. It is therefore essential to find the right measure, where the heating in the second stage does not yet couple into the supersonic core but raises the temperature of the cold gas layer and thereby increases the integral of the velocity of the flow.

Radius resolved plume characteristics are measured by a time-of-flight electric probe and a Pitot probe. The data are compared to the integral plasma power measured by a cavity calorimeter.

After introducing the thruster principle, the present paper presents the setup of the ground test facility, the measurement devices, and the methodolgy to determine plasma temperature from total pressure and velocity. The data will then be compared by an equilibrium approach.

*Research Engineer, now with German Aerospace Center (DLR), Institute of Structures and Design, Stuttgart, Germany, hannah.boehrk@dlr.de .

†Professor, now President of the Universität Hamburg.

II. Thruster concept

As mentioned above, TIHTUS consists of an arcjet thruster (first stage) and an inductively heating afterburner (second stage). A view of the plasma thruster TIHTUS is shown in figure 1. The second stage consists of a discharge tube and a coil spun around it as part of a resonance circuit. The inductively heated plasma generator (IPG) is used as the afterburner since in induction heating the power is coupled into the plasma at a near-coil position due to the skin-effect [9]. In an arcjet plume, as mentioned in the introduction, this is where the cold gas layer is located. The plasma jet being ejected from the arcjet is thus expanded into the quartz discharge tube. The alternating RF-current in the coil induces an oscillating, mostly azimuthal, magnetic field inside the tube. This field initiates an electric discharge in the propellant oriented in the opposite direction of the coil current. The free electrons contained in the plasma from the thermal arcjet are accelerated by the electric field and by means of collisions they transfer their induced power to the atoms and molecules. RF-power is thus coupled into the plasma.

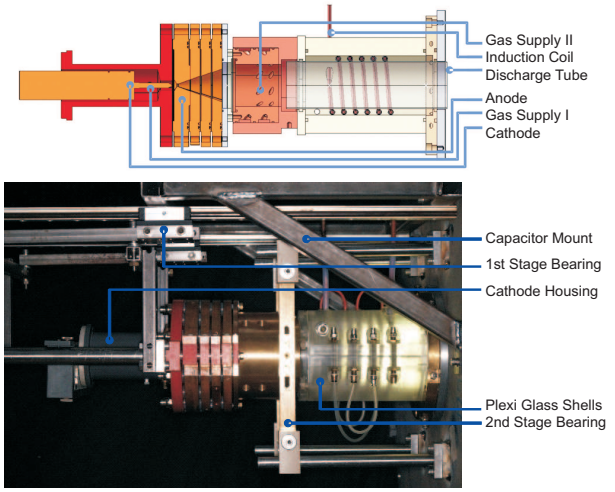

Figure 1 Set-up of TIHTUS.

The thruster is operated as a water-cooled model using hydrogen as propellant. Power may be coupled into the arc-heated (DC) or the inductively heated (RF) stage. The principal question is whether it is possible to specifically heat the outer edges of an arcjet plume so that higher exhaust velocity can be attained. Of course, a dependency on the power staging between the two thruster stages is expected. As is a dependency on the gas mass flow rate staging. Gas flow through the arc heated stage is expanded first into the injection head of the inductive, second stage where a swirl gas flow can be admixed. Each operational condition is therefore referred to as T $P_{DC}|P_{RF}$-$\dot{m}_{DC}|\dot{m}_{RF}$ throughout this paper. The investigated conditions are listed in table 1. They include a variety of conditions where at constant mass flow staging (300|0 mg/s) the power staging is varied while keeping the total power input at 50 kW. In the second variety, mass flow staging, where the total mass flow always adds up to 300 mg/s, is varied at constant power staging (25|25 kW).

Table 1 Nomenclature for operational condition.

	P_{DC} [kW]	P_{RF} [kW]	$\dot{m}_{DC}$ [mg/s]	$\dot{m}_{swirl}$ [mg/s]
T 50|00-300|0	50	0	300	0
T 25|25-300|0	25	25	300	0
T 20|30-300|0	20	30	300	0
T 25|25-200|100	25	25	200	100
T 25|25-100|200	25	25	100	200

III. Experimental Environment

The TIHTUS ground test facility consists of the two plasma thuster stages and the vacuum chamber measuring 3 m in length and 2 m in diameter. Installed are a gas supply system, water-cooling system and a data acquisition system. The lid of the vacuum chamber carries the thruster. The rear end of the chamber is connected to the IRS vacuum pump system, the total suction power of which amounts to 6000 m^3/h at atmospheric pressure or 250 000 m^3/h at 10 Pa.

TIHTUS' first stage is a water-cooled arcjet thruster foreseen for up to 100-kW operation. It is supplied by a 6-MW DC-power supply. The second stage is connected to a 180-kW radio-frequency power supply and the external resonance circuit can be operated at frequencies ranging from 0.5 to 1.5 MHz.

Both parts of the thruster are water-cooled at present. Therefore, thermal powers such as tube cooling power loss or resonant circuit power are surveyed using resistance thermometers. They are electrically sealed and installed at an acceptable distance from the plasma source to prevent disturbing signals from the RF-field. Additionally, the cooling water flow rates are measured. However, at a further stage of development, the strategy foresees building the plasma source in a radiation-cooled design, promising an additional gain in specific impulse.

For gas dynamic plume investigation, a two-axis table is installed inside the vacuum tank on which probes can be mounted. Moreover, optical access is provided by portholes.

Thrust was also investigated and is presented in Ref. [10].

A. Cavity Calorimeter

A cavity calorimeter was developed to determine thermal plasma power [11]. The plasma ejected from the thruster enters the cone-shaped copper cavity shown in figure 2. The diameter of the entrance aperture is 120 mm, which is approximately 25% larger than the plasma beam. The distance between the calorimeter and the plasma outlet of TIHTUS is 70 mm. The distance must be large enough so that the discharge behavior of the plasma thruster is not disturbed. The calorimeter is made of copper due to the material's very high specific heat conductivity. The copper walls are thus heated by radiation, convection, and wall-recombination. The entire cavity is equipped with spiral copper tubes on the outside that guide the

Figure 2 Cavity calorimeter of IRS.

cooling water, see figure 2. The water cools the copper wall so that the plasma is completely cooled and the entire power of the plasma is transferred to the cooling water. The plasma power P_{Pl} is then determined according to [12]

$$P_{Pl} = \dot{m}_{coolant} c_{p,coolant} \left(T_{out} - T_{in}\right). \qquad (1)$$

B. Pitot Probe

The total, or Pitot, pressure p_{tot} is the pressure present in the foremost stagnation point of a body inserted into a plasma column, such as a Pitot probe. Within the probe the deceleration of the flow takes place isentropically. The pressure measured at the end of a Pitot tube, therefore, corresponds to the total pressure in the stagnation point in front of the tube opening. At a Mach number of $Ma \geq 1$, this is the plenum pressure just behind an imaginary vertical, ideal bow shock.

Figure 3 Pitot probe.

Mach number is defined as

$$Ma = \frac{v}{a} = \frac{v}{\sqrt{\kappa R T}} \qquad (2)$$

with the speed of sound a , the isentropic exponent κ, and the specific gas constant R. Depending on Mach number, in the stagnation point a total pressure is formed so that

$$\frac{p_{tot}}{p_{stat}} = \left(\frac{\kappa+1}{2} Ma^2\right)^{\frac{\kappa}{\kappa-1}} \left(2\frac{\kappa}{\kappa+1} Ma^2 - \frac{\kappa-1}{\kappa+1}\right)^{\frac{1}{1-\kappa}} \qquad (3)$$

in supersonic and

$$\frac{p_{tot}}{p_{stat}} = \left(1 + \frac{\kappa-1}{2} Ma^2\right)^{\frac{\kappa}{\kappa-1}}. \qquad (4)$$

in subsonic flow [8]. The isentropic exponent κ is a function of temperature. It was shown by Laure, that a deviation has only little influence on the result of Mach number from equation (3) [13]. The data presented here are furthermore based on the assumption that the ambient pressure in the vacuum tank is imposed on the plasma plume. This assumption is also supported by Refs. [14] and [15].

The Pitot probe used in the present case is of European standard geometry (flat nose, 50 mm body diameter, rounded edge) with a measurement orifice of 26 mm diameter. It is depicted in figure 3.

C. Electric Time-of-Flight Probe

For the measurement of the plasma velocity v_∞, electric time-of-flight probes are applied. Electric probes are electrically conductive measurement devices exposed to a plasma. A double probe has two electrodes with a voltage applied between them. Due to an electrically conductive plasma passing between the electrodes, a current flows and can be measured.

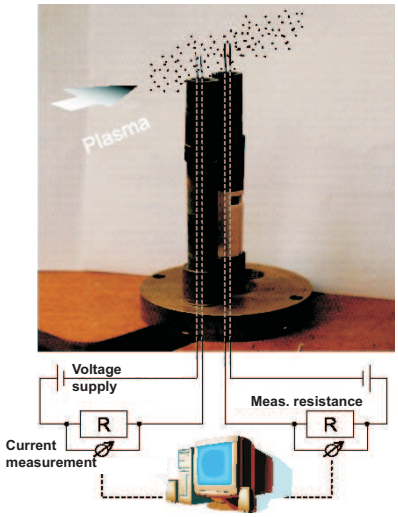

Figure 4 Electric time-of-flight probe setup.

The principle for plasma velocity measurement, depicted in figure 4, is based on the axial offset of two double probes. The current flow between either pair of electrodes, as depicted in figure 5, shows fluctuations in the plasma which translate with plasma velocity from the first to the second double probe.

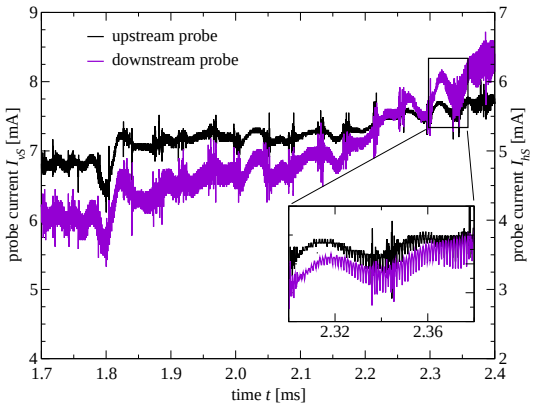

Figure 5 Probe data from operational condition T 25|25-100|200.

The electrodes are of tungsten wire with a diameter of 0.5 mm and the two double probes have an axial offset of 26 mm.

The voltage induced into the electrodes by the RF magnetic field is dependent upon the magnetic field strength B and the projected area A_{proj} of the electrodes according to

$$V_{ind} = \dot{B} A_{proj} + B \dot{A}_{proj} \,. \tag{5}$$

Consequently, the probes are arranged so that all four cylindrical probes of the two double probes are axially aligned with the plume axis so that the projected area is minimized.

IV. Measurement Results

As was described in chapter II, in TIHTUS, electric power can be applied to either the arc heated stage, the inductively heated stage, or to both stages. Also, the ratio of the gas flow through either stage can be varied. The five operating conditions of table 1 were investigated. They include a variation of power staging for a gas flow relation of 300|0 mg/s and a variation of mass flow staging for constant power staging of 25|25 kW.

The radial profiles of total pressure and plasma flow velocity at an axial position of x=200 mm from the thruster exit are measured by means of a Pitot probe and a time-of-flight electric probe, respectively.

A. Pitot Pressure

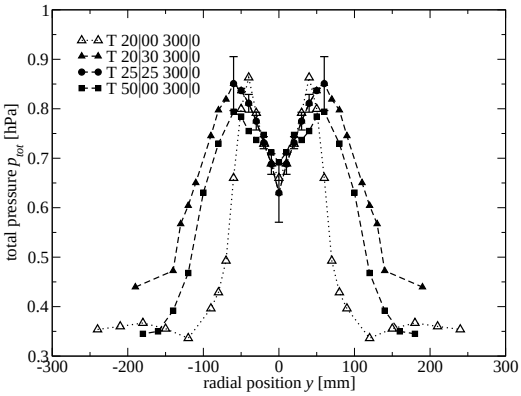

Figure 6 Pitot pressure at variation of power partitioning.

Figure 6 shows Pitot pressure in the plane perpendicular to the plume exhaust direction with a mass flow rate of 300 mg/s through the arcjet thruster stage. For proof of reproducibility, the measurement points were detected twice and averaged values are presented here. Error bars in the graphs include the standard deviation of the mean value and the uncertainty of the pressure transducer. The maxima at excentric position originate from the plasma flow through the discharge tube instead of a diverging nozzle. The curve marked with hollow triangles represents only arc heated stage active at 20 kW. It shows maxima at excentric position, while the plume is quite narrow. Black triangles mark the same arcjet power with second stage power added to it. It becomes evident, that the power of the inductively heated stage is coupled into the plasma annularly at excentric position. For reasons of clarity in the figure, error bars are marked only in the curve for the condition T 20|30-300|0.

The black symbols represent conditions with power staging adding up to 50 kW each. At the plume center, it can be observed that higher total pressure is produced with increasing arc power. The highest maxima representing a total pressure of 0.85 hPa are achieved with 20 kW supplied from the arc heating stage and 30 kW coupled into the plume by inductive heating. The same condition shows the widest plume diameter. This can be interpreted as the most power coupled into the plasma at coil-near position. However, the smallest diameter is *not* reached at pure arc heating with 50 kW but with 25 kW arc and 25 kW inductive heating.

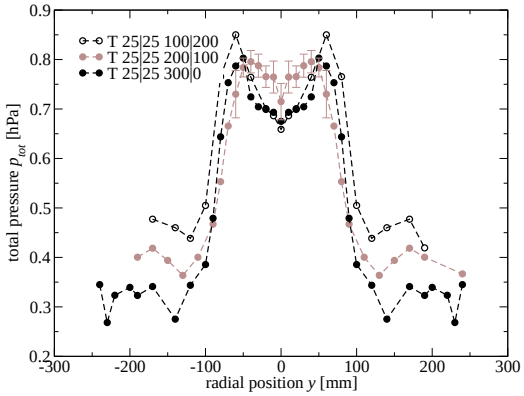

Figure 7 Pitot pressure at variation of mass flow rate partitioning.

For a power staging of 25|25 kW, a gas flow variation was also conducted. The Pitot pressure graphs are presented in figure 7. From the edges of the plume, it can be seen that according to the measurement condition and the mass flow staging, the ambient pressure in the tank varies between 0.34 und 0.4 hPa. In the second stage, the gas flow is injected radially as swirl gas. It is observed that the more gas is injected as swirl gas, the higher the ambient pressure. The diameter of the plasma plume, however, does not remarkably change with varying mass flow staging. Total pressure maxima of 0.85 hPa are reached for 100|200 mg/s.

From these measurements, the highest integral of total pressure is reached with T 20|30-300|0. The data compared well to thrust measurements as elaborated in Ref. [10].

B. Velocity

In the figures 8 and 9, plasma velocities investigated with electric time-of-flight probes are depicted. Note that measurements could only be taken around the plume center, where ionization of the plasma was high enough to have a current flow through the plasma and the electric probes. Profiles were able to be recorded out to a radial distance of 110 mm from the plume center.

At each radial position five pairs of curves were recorded. The velocities determined from their cor-

relation were then averaged. Error bars denominate the standard deviation of the mean value and the uncertainties of measurement of the electrode distance.

Figure 8 represents the variation of power staging according to the pressure data presented above. The curves do not have the excentric maximum shape as the Pitot pressure curves. They demonstrate a maximum at centric position. The center values, as according to the Pitot center values increase with increasing first stage power. Power partitioning of 25|25 kW reaches almost the maximum velocity of 9224 m/s in the plume center that were reached by the one of 50|0 kW with an addition of power at the plume edge. Of much smaller amount is the maximum of the power staging with 20|30 kW. This means that when too little power is applied by the first stage, ionization is not high enough for the induction coil to efficiently couple power into the plasma. Furthermore, velocity decreases while the profile gains in diameter.

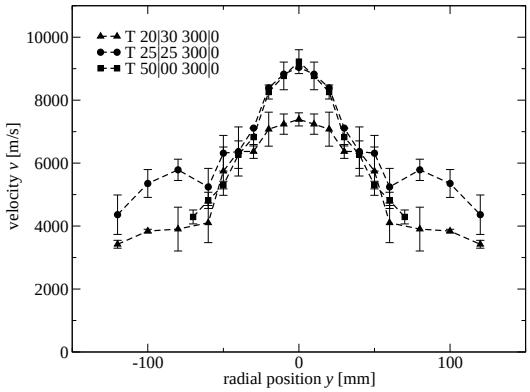

Figure 8 Velocity at variation of power partitioning.

At maintained power ratio of 25|25 kW, the gas flow variation shows that with pure flow through the arcjet, a maximum is formed in the plume center. However, for increasing swirl gas flow, the maxima become excentric. This is most extreme for 100 mg/s of hydrogen fed through the arcjet and 200 mg/s fed through the injection head. The highest local velocities of >10,300 m/s are reached with 200 mg/s of hydrogen fed through the arcjet and 100 mg/s fed through the injection head. The plume centers show an increase in velocity with increasing arcjet flow.

C. Plasma Power

It was shown in Ref. [7] that plasma power can be estimated from operation supervisory data with an accuracy of below 10% according to the method described.

For the second – inductive – stage, a loss was reported by Herdrich which is referred to as the "neutral gear power" [11]. Neutral gear power is lost to the components of the facility, e.g. in the form of electromagnetic emission or to the oscillator tube, amongst others. The neutral gear power P_{ng} can be assessed during operation without a plasma load. Thus, only a part of the anode power P_A is induced into the plasma as $P_{ind}=P_A - P_{ng}$. Again, from the power induced

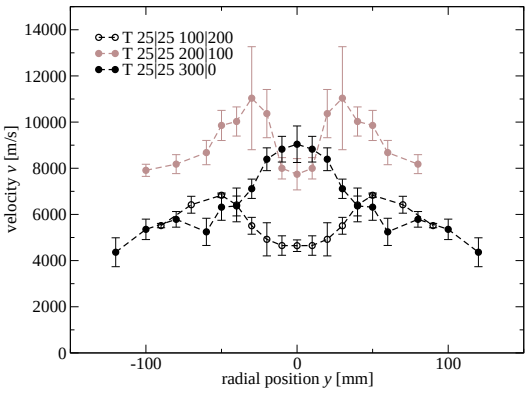

Figure 9 Velocity at variation of mass flow rate partitioning.

into the plasma, a part is lost to the cooling water, indicated by $P_{th,RF}$ and measured as described above

$$P_{Pl,RF} = P_A - P_{ng} - P_{th,RF}. \quad (6)$$

Figure 10 shows a principle of the two-stage thruster TIHTUS. Sketched are the gas flow, the input power to each stage, as well as the power losses. According to the figure, the plasma power must yield

$$P_{Pl} = P_{el,DC} + P_A - P_{th,DC} - P_{th,RF} - P_{ng}. \quad (7)$$

In order to prove equation (7) true, the results are compared to the plasma power measured with the calorimeter described above. Table 2 shows the results and that this method of determining plasma power lies within a range of precision of 10% for hydrogen operation.

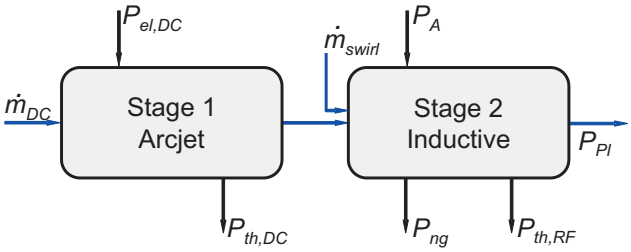

Figure 10 Staging principle

The general definition of efficiency is $\eta = \frac{useable\ power}{supplied\ power}$. Thus, in the present case, thermal efficiency is, according to Fig. 10, defined as

$$\eta_{th,tot} = \frac{P_{Pl}}{P_{el,DC} + P_A}. \quad (8)$$

Table 2 Plasma power and thermal efficiency: directly measured and determined from operational data.

	$P_{Pl,cal}$ [kW]	$P_{Pl,Eq.(7)}$ [kW]	error [%]	$\eta_{th,cal}$ [%]
T 50|00-300|0	25.56	25.56	0	51.04
T 25|25-300|0	20.39	22.16	8.7	40.67
T 20|30-300|0	21.16	21.73	2.7	41.73
T 25|25-200|100	21.08	19.99	5.2	42.87
T 25|25-100|200	21.32	19.54	8.4	42.31

The part of the plasma power that can be used for thrust depends on the frozen flow losses and on the nozzle efficiency.

V. Interpretation

In this section, it will be shown how the radially resolved data can be combined and a *plasma temperature* can be derived. However, this has to be done under the assumption of thermal and chemical equilibrium. Whether comsideration of thernmodynamic equilibrium is admissible will be cross checked by deriving plasma enthalpy from the probe data and comparing it to the plasma enthalpy measured with the calorimeter. It will be shown that the data compare well.

A. Temperature

In the present elaboration, the plume of the two-stage TIHTUS thruster is investigated by a Pitot pressure and an electric time-of-flight probe. A novel method was introduced in [10], in which from total pressure and velocity, temperature is deduced. It shall be briefly reported, here.

The isentropic exponent κ and the specific gas constant R are each dependent on temperature. In the present study, their values are taken from Ref. [16] based on a plasma composition model assuming thermodynamic equilibrium. Transferring eq. (2) to a function for velocity v of temperature T results in

$$v^2 = Ma^2\kappa(T)R(T)T\,. \tag{9}$$

Figure 11 shows the velocity of a plasma plume as derived from eq. (9) for a total pressure ratio measured at T 50|00-300|0.

For the same operating point and position, the velocity measured by electric probes is marked in the graph as a horizontal line. In the figure, the velocity derived from Pitot probe measurement for a variety of temperatures and the velocity measured with electric probe intersect. Namely, at the temperature for the pressure ratio of which the "true" velocity was measured by the electric probes. This temperature is the plasma temperature at the position and the operating position. This means that the local temperature is derived from velocity an total pressure measurements while only two assumptions have to be made: a perpendicular, ideal bow shock in front of the Pitot probe and plasma fluctuations measured by the electric probes moving with plasma veocity. Furthermore, isentropic exponent and specific gas constant were calculated from a model considering thermo-chemical equilibrium [16].

In the framework of the present measurement campaign, a radial profile of plasma velocity was measured for the five operating conditions of table 1. Hence, for each point of measurement in each radial profile the temperature is determined from Pitot probe and electric time-of-flight measurements. It is subject to uncertainties of the determination of total pressure and velocity. The uncertainties are given as error bars in figure 12.

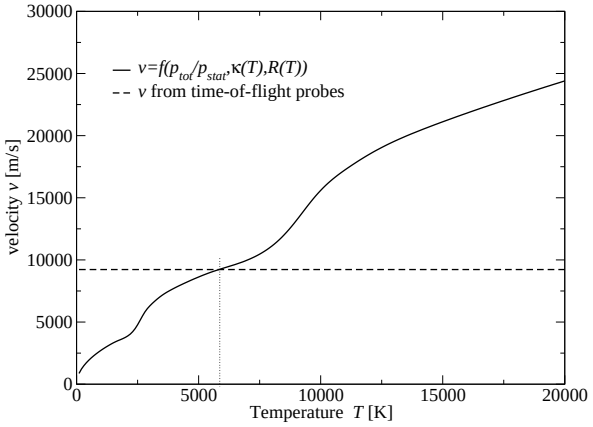

Figure 11 Scheme of temperature determination method.

By means of this method, the temperature is derived from Pitot pressure and plasma velocity. For the operating conditions T 50|00-300|0, T 25|25-300|0, and T 20|30-300|0, the temperatures deduced are depicted in figure 12. The method was compared to temperatures results of thermo-chemical non-equilibrium consideration and it was found that a good agreement of below 30% is reached with the method [17].

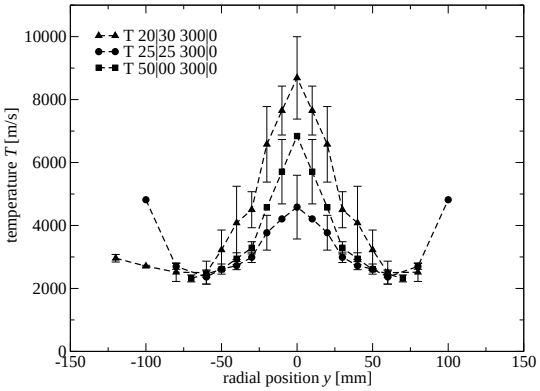

Figure 12 Temperature at variation of power partitioning.

It becomes evident from figure 12 that for all operating conditions using pure central gas flow at 300 mg/s the temperature profile is very simlar at any power staging. This indicates that the thermal efficiency of the coupling of the inductive, second stage into the plasma is high. The highest temperature of 8689 K is reached under condition T 20|30-300|0, while at T 50|00-300|0 the temperature is approximately 1500 K lower. The lowest temperature on the plume axis is reached at T 25|25-300|0. Towards the plume edge, they all fall down to about 2300 K. Remember that the measurement was not possible to be conducted all the way out the actual plume edge since the degree of ionisation was not high enough for the electric probes to measure reliable values.

B. Enthalpy

Analoguous to Ref. [18], the enthalpy under consideration of thermodynamic equilibrium in case of hydrogen operation yields

$$h \;=\; \frac{1}{2}v_\infty^2 + c_{p_{rot,tr}}T_\infty \tag{10}$$

$$+\xi_{H_2} h_{vib,H_2} + \xi_H h_{dis} + \xi_{H^+} \left(h_{dis} + h_{ion}\right),$$

where according to Ref. [19] $c_{p_{rot,tr}}$ yields

$$c_{p_{rot,tr}} = \frac{\bar{f}+2}{2}\frac{\Re}{\bar{M}}. \tag{11}$$

and

$$h_{vib,H_2} = \frac{\frac{\Re}{M_{H_2}}\theta_{vib}}{e^{\frac{\theta_{vib}}{T_{vib}}} - 1}, \tag{12}$$

At the axial position x=200 mm downstream of the nozzle of TIHTUS, from the measurements presented above, the locally resolved profiles of T and v_∞ are known. Although velocity data could only be detected up to a radius of 110 mm from the plume center, total pressure shows that the plume is remarkably larger, namely, up to a radius of 150 mm. Temperature and velocity are therefore extended by a fit curve according to Abramovich giving universal radial profiles for turbulent free jets in the form of [20]

$$v = v_a \left(1 - \left(\frac{r}{R_S}\right)^{3/2}\right)^2. \tag{13}$$

The velocity maximum at the plume center is named v_a and r stands for radial position while R_S denominates the plume radius. Figure 13 compares the measured velocity of condition T 50|00-300|0 to the fit-function above. It can be seen that the theory applies well to the plasma characteristics of TIHTUS when the thruster is operated with a mass flow staging of 300|0 mg/s.

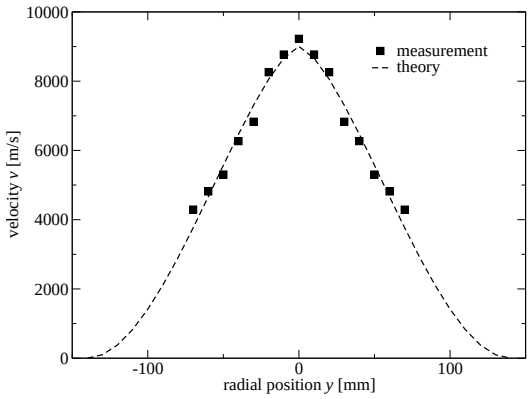

Figure 13 Velocity profiles of T 50|00-300|0: measured and fitted according to the theory of Abramovich.

Fasoulas has added a universal radial profile for the specific enthalpy in the form of

$$h = h_a \left(1 - \left(\frac{r}{R_S}\right)^{3/2}\right)^3. \tag{14}$$

Figure 14 shows the enthalpy deduced from eq. (14) and compares them to the pure equilibrium enthalpy from eq. (11) deduced from measured velocity and total pressure values. The bulk plasma enthalpy at T 50|00-300|0 yields

$$h_{Pl,cal} = \frac{P_{Pl}}{\dot{m}} = 86.67\,\mathrm{MJ/kg} \tag{15}$$

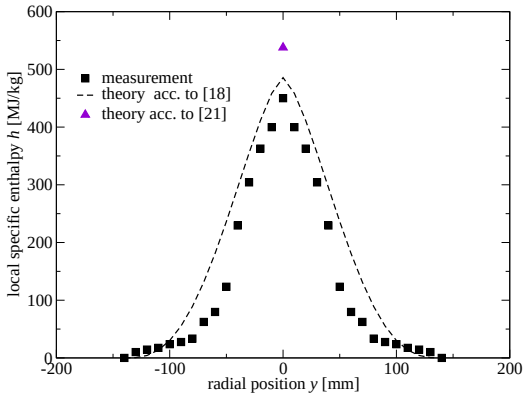

Figure 14 Enthalpy profiles of T 50|00-300|0: fitted from semi-empirical model [18] and derived with equilibrium model from measurement data.

and is known from the plasma power measured with the calorimeter. The enthalpy at the plume center h_a in eq. (14) must, since, be chosen so that the integral of the enthalpy profile across the plume cross section

$$h_{Pl} = \int_A h dA = \frac{1}{A}\sum_i h_i. \tag{16}$$

yields the same value.

It can be seen from figure 14 that the form and trend of the turbulent free stream's enthalpy is in agreement for both Fasoulas' semi-empiric theory and thermodynamic equilibrium considerations. This show that equilibrium considerations are admissible. The curve's integral differs with 59.12 MJ/kg only 30% from that of 86.67 MJ/kg measured with the calorimeter.

In both of the above cases it is assumed that the mass flow distribution is homogenuous throughout the entire plume section. In order to avoid having to make this assumption, Löhle derived radially resolved specific enthalpy according to eq. 14, yielding [21]

$$h = \frac{h_a v_a}{\dot{m}}\frac{pA}{RT}\left(1 - \left(\frac{r}{R_S}\right)^{3/2}\right)^5 \tag{17}$$

The value of h_a, i.e. that of the plume center, is also depicted in figure 14. It lies 10% above the semi-empiric model of Fasoulas, may be indicating that $\dot{m}=\frac{p}{RT}vA$ has increased while the plasma travelled the 200 mm from the thruster exit to the probes, e.g by entrainment of ambient air. That this entrainment takes place was was shown before by Fasoulas [18, 22].

Acknowledgement

The authors would like to thank Dr. Thomas Stöckle for initiating the idea of temperature deduction, Dr. Stefan Löhle for fruitful discussions on plasma enthalpy and their students Melanie Lücke und Markus Mayer for their contribution to the presented experiments.

They also thank their colleague Uwe Bauder for kindly presenting these interesting results at the 30^{th} IEPC in Florence, Italy.

References

[1] Bonneville, J.M., "High-Frequency Supersonic Heating of Hydrogen for Propulsion," *AIAA Electric Propulsion Conference*, Colorado Springs, CO, 1963.

[2] Wallner, L.E., Czika, J., "Arc-Jet Thrustor for Space Propulsion," Tech. rep., NASA, Lewis Research Center, Cleveland, OH, 1965.

[3] Auweter-Kurtz, M., *Lichtbogenantriebe für Weltraumaufgaben*, B.G. Teubner, Stuttgart, 1992.

[4] Böhrk, H., Schmidt, T., Auweter-Kurtz, M., "Flexible Piloted Mars Missions using the TIHTUS Engine," *Aerospace Science and Technology*, Vol. 11, No. 2-3, 2007, pp. 211–221.

[5] Böhrk, H., Auweter-Kurtz, M., "Preliminary Results of TIHTUS Operation," *AIAA 2007-5158*, Sacramento, CA, Jul. 2006.

[6] Böhrk, H., Laure, S., Auweter-Kurtz, M., "Feasibility Study of Application of ATTILA to In-Space Propulsion for Piloted Missons," *IAC-04-S.4.03*, Vancouver, Kanada, Okt. 2004.

[7] Böhrk, H., Auweter-Kurtz, M., "Efficiency Analysis of the Two-Stage Thruster TIHTUS," *Journal of Thermophysics and Heat Transfer*, 2007, under review, also presented as conference paper AIAA 2007-4149.

[8] Liepmann, H.W., Roshko, A., *Elements of Gasdynamics*, John Wiley and Sons, Inc., New York-London, 3rd ed., 1960.

[9] Eckert, H.U., "The Induction Arc: A State-of-the-Art Review," *Journal of High Temperature Science*, Vol. 6, 1973, pp. 99–134.

[10] Böhrk, H., Auweter-Kurtz, M., "Thrust Measurement of the Two-Stage Electric Thruster TIHTUS by a Baffle Plate," *Journal of Propulsion and Power*, 2007, under review, also presented as conference paper AIAA 2007-5297 "TIHTUS Thrust Measurement with a Baffle Plate".

[11] Herdrich, G., Auweter-Kurtz, M., Kurtz, H., "Operational Behavior of Inductively Heated Plasma Source IPG3 for Entry Simulations," *Journal of Thermophysics and Heat Transfer*, Vol. 16, No. 3, 2002, pp. 440–449.

[12] Scott, C.D., "Survey of Measurements of Flow Properties in Arc Jets," *5th Thermophysics and Heat Transfer Conference*, Seattle, WA, Jun. 1990, AIAA 90-1765.

[13] Laure, S., *Experimentelle Simulation der Staupunktströmung wiedereintretender Raumflugkörper und deren Charakterisierung mittels mechanischer Sonden*, Dissertation, Universität Stuttgart, Fak. Luft- und Raumfahrttechnik, 1998.

[14] Laure, S., Auweter-Kurtz, M. Fasoulas, S., Habiger, H., Schönemann, A., "Experimentelle Simulation einer hochenthalpen Luftströmung im Plasmawindkanal," *Jahrbuch der deutschen Gesellschaft für Luft- und Raumfahrt*, Vol. 3, DGLR, Erlangen, 1994.

[15] Abramovich, G.N., *Theory of Turbulent Jets*, MIT Press, 1963, p269.

[16] Patch, R.W., "Thermodynamic Properties and theoretical Rocket Performance of Hydrogen to 100,000 K and $1.01325\times10^8\,\mathrm{N/m^2}$," Tech. rep., NASA, Lewis Research Center, Cleveland, 1971.

[17] Mayer, M., *Eine Methode zur Temperatur- und Schubbestimmung für elektrische Raumfahrtantriebe aus gasdynamischen Sondenmessungen*, Diplomarbeit, Institut für Raumfahrtsysteme, Universität Stuttgart, 2007.

[18] Fasoulas, S., *Experimentelle und theoretische Charakterisierung einer hochenthalpen Stickstoffströmung zur Wiedereintrittssimulation*, Dissertation, Universität Stuttgart, Fak. Luft- und Raumfahrttechnik, Jun. 1995.

[19] Vincenti, W.G., Kruger, C.H., *Introduction to Physical Gas Dynamics*, John Wiley & Sons Inc., New York, 1965.

[20] Abramovich, G.N., *Theory of Turbulent Jets*, MIT Press, 1963.

[21] Loehle, S., *Untersuchung von Wiedereintrittsplasmen mit Hilfe laserinduzierter Fluoreszenzmessungen*, Dissertation, Universität Stuttgart, Fak. Luft- und Raumfahrttechnik, 2006.

[22] Fasoulas, S., Sleziona, C., Auweter-Kurtz, M., Habiger, H., Laure, H. and Schönemann, A., "Characterization of a Nitrogen Flow within a Plasma Wind Tunnel," *Journal of Thermophysics and Heat Transfer*, Vol. 9, No. 3, 1995, pp. 422–431.